


Onset and maturation of Asian summer monsoon precipitation reconstructed from intra-annual tree-ring oxygen isotopes from the southeastern Tibetan Plateau

Chenxi Xu^{a,b,*} , Haifeng Zhu^c, S.-Y. Simon Wang^d, Feng Shi^{a,b}, Wenling An^{a,b}, Zhen Li^e, Masaki Sano^f, Takeshi Nakatsuka^e, Zhengtang Guo^{a,b,g}

^aKey Laboratory of Cenozoic Geology and Environment, Institute of Geology and Geophysics, Chinese Academy of Sciences, Beijing 100029, China

^bCAS Center for Excellence in Life and Paleoenvironment, Beijing 100044, China

^cKey Laboratory of Alpine Ecology and Biodiversity, Institute of Tibetan Plateau Research, Chinese Academy of Sciences, Beijing 100085, China

^dDepartment of Plants, Soils, and Climate, Utah State University, Logan 84322, Utah, USA

^eGraduate School of Environment Studies, Nagoya University, Nagoya 464-8601, Japan

^fFaculty of Human Sciences, Waseda University, 2-579-15 Mikajima, Tokorozawa 359-1192, Japan

^gUniversity of the Chinese Academy of Sciences, Beijing 100049, China

*Corresponding author at: Institute of Geology and Geophysics, Chinese Academy of Sciences, No. 19, Beitucheng Western Road, Chaoyang District, Beijing 100029, China. E-mail address: cxxu@mail.iggcas.ac.cn (C. Xu).

(RECEIVED December 21, 2019; ACCEPTED March 13, 2020)

Abstract

We present a long-term seasonal tree ring cellulose oxygen isotope ($\delta^{18}\text{O}_c$) time series created by analyzing four segments (S1, S2, S3, and S4) per year during the period of 1951–2009 from southeastern Tibetan Plateau. This intraseasonal $\delta^{18}\text{O}_c$ reveals the onset and mature phase of the summer monsoon precipitation in this region. Analysis indicates that the $\delta^{18}\text{O}_c$ of S1 has the strongest correlation with precipitation during the regional monsoon onset (29–33 pentads, May 21–June 10, $r = -0.69$), and the $\delta^{18}\text{O}_c$ values for S2, S3, and S4 correlate strongly with June, July, and August precipitation, respectively. Combined $\delta^{18}\text{O}_c$ of S2, S3, and S4 shows the most robust correlation ($r = -0.82$) with the mature-phase monsoon precipitation (June–July–August, JJA), passing rigorous statistical tests for calibration and verification in dendroclimatology. These results demonstrate the feasibility in using long-term intraseasonal $\delta^{18}\text{O}_c$ to reconstruct the Asian summer monsoon's intraseasonal variations.

Keywords: Tree-ring oxygen isotopes; *Abies georgei*; Monsoon onset and mature phase; Asian summer monsoon; Southeastern Tibetan Plateau

INTRODUCTION

The variability of the Asian summer monsoon ranges from intraseasonal variation to thousands of years, driven by different mechanisms for different time scales (Wang et al., 2017). Investigating Asian summer monsoon variations across time scales is helpful for understanding current monsoon changes and predicting possible future changes. The onset of the summer monsoon is crucial to society and ecology, not only because it signifies the end of the dry season, but also due to its link to extreme weather. The monsoon in Asia

experiences a rapid warming in the surface air mass, followed by episodic increases in humidity with occasional thunderstorms, and, subsequently, the steady monsoon rains. That last phase, with its combined increases in air temperature and humidity, forms a brief period of elevated convective instability that is prone to lightning, rainstorms, and associated flooding (Joseph et al., 1994; Ullah and Shouting, 2013; Wang et al., 2011; Siingh et al., 2015; Li et al., 2019). Depending on its location across monsoonal Asia, the rainy season may be punctuated by one or two “break” phases with a notable decrease of rainfall; this is due to the evolution of tropical intraseasonal oscillations (Krishnan et al., 2006; Kulkarni et al., 2011) and/or the passage of the North Pacific subtropical anticyclone (Wang et al., 2016). Reconstructing the evolution of monsoonal precipitation has been challenging, despite the rich literature of using tree rings to reconstruct the seasonal monsoon rains.

Cite this article: Xu, C., Zhu, H., Wang, S.-Y. S., Shi, F., An, W., Li, Z., Sano, M., Nakatsuka, T., Guo, Z. 2021. Onset and maturation of Asian summer monsoon precipitation reconstructed from intra-annual tree-ring oxygen isotopes from the southeastern Tibetan Plateau. *Quaternary Research* 103, 139–147. <https://doi.org/10.1017/qua.2020.28>

Tree ring-based precipitation reconstructions are usually seasonal or annual, because annual tree growth or isotopes were affected by climate in the current or previous growing seasons (Cleaveland et al., 2003; Shao et al., 2005; Treydte et al., 2006; Yang et al., 2014; Xu et al., 2018). Occasionally, tree-ring widths and isotopes can be used for depicting the intraseasonal precipitation, for example, May–June precipitation reconstruction based on tree-ring width and oxygen isotope (Touchan et al., 2007; Xu et al., 2019a). Earlywood and latewood represent the different growth periods, and a careful parsing of the signals can extract intraseasonal precipitation (Griffin et al., 2013; Young et al., 2015). However, few studies have obtained a robust reconstruction of monsoon precipitation during its onset or peak phase, and none have done a reconstruction of these in combination for the same location.

Tree ring cellulose oxygen isotope ($\delta^{18}\text{O}_c$) is mainly controlled by relative humidity and the precipitation oxygen isotope (Roden et al., 2000). Higher relative humidity may reduce evapotranspiration, resulting in less enriched leaf-water oxygen isotope and $\delta^{18}\text{O}_c$, and the precipitation oxygen isotope signal can be transferred into $\delta^{18}\text{O}_c$ (Roden et al., 2000). Monsoon season relative humidity is usually related to precipitation amount in monsoonal Asia, so higher precipitation is associated with reduced $\delta^{18}\text{O}_c$. A negative relationship between precipitation amount and precipitation oxygen isotope ratio in the monsoon season has been identified in Asian summer monsoon areas (Dansgaard, 1964; Vuille et al., 2003; Kurita et al., 2009), and higher monsoon precipitation is correlated with depleted $\delta^{18}\text{O}_c$. Therefore, $\delta^{18}\text{O}_c$ in monsoonal Asia is a demonstrated proxy for monsoon season precipitation (Grießinger et al., 2011; Sano et al., 2013; Xu et al., 2013, 2015).

It has been proposed that increasing the temporal resolution in $\delta^{18}\text{O}_c$ can potentially reveal monthly precipitation; for example, Xu et al. (2016) found that $\delta^{18}\text{O}_c$ deposited in July is highly correlated with July precipitation. Previous studies using intraseasonal $\delta^{18}\text{O}_c$ from different tree species also showed how the seasonal evolution of monsoonal precipitation can be reconstructed based on relatively limited years of $\delta^{18}\text{O}_c$ data (Managave et al., 2010a, 2010b; Xu et al., 2016; Zeng et al., 2016, 2017). However, the use of intra-annual $\delta^{18}\text{O}_c$ analysis for the rigorous reconstruction of monsoon onset and peak precipitation has not been attempted.

In this study, we built seasonal $\delta^{18}\text{O}_c$ time series for *Abies georgei* on the southeastern Tibetan Plateau by dividing each ring into four segments (S1, S2, S3, S4) and measuring the $\delta^{18}\text{O}_c$ in each segment. We then used seasonal $\delta^{18}\text{O}_c$ variations to reconstruct the onset and mature phase of summer monsoon precipitation.

MATERIALS AND METHODS

Sampling site and oxygen isotope analysis

We present the long-term seasonal $\delta^{18}\text{O}_c$ time series from one *A. georgei* core (sample number: XC02a) in the southeastern Tibetan Plateau (Fig. 1). *Abies georgei* and *Hippophae*

tibetana grow on the terminal moraines in Xincuo (30.09° N, 94.27° E, 3930 m above sea level), and we collected samples using 5 mm increment borers. The samples were dried, polished, and cross-dated.

A modified plate method was used to extract α -cellulose (Xu et al., 2011, 2013). We cut the core sample into 1-mm-thick wood plates for chemical treatment. We removed lignin, hemicellulose, lipids using a 17 wt% NaOH solution, an acidified NaClO₂ solution, toluene and ethanol (1:1), respectively. After cellulose extraction, the cellulose plate was dried in an oven for 2 hours. The separation of each ring from the cellulose plate was performed under a binocular microscope. Each cellulose ring was divided into four parts with the same width, a method that follows Managave et al. (2010a); these four components of the cellulose ring are referred to as S1, S2, S3, and S4, representing cellulose formed during each fraction of the growing season. To compare the climatic response of seasonal $\delta^{18}\text{O}_c$ with annual $\delta^{18}\text{O}_c$, the annual $\delta^{18}\text{O}_c$ chronology based on four trees (XC2, XC6, XC12, and XC14) that was produced by Xu et al. (2019b) was used in this study and is termed “annual(4).”

We wrapped 80–260 μg of each α -cellulose sample in silver foil for isotope measurements. Tree ring cellulose samples were converted into CO gas by a pyrolysis-type elemental analyzer (TC/EA) at 1375°C, and then oxygen isotope ratios ($^{18}\text{O}/^{16}\text{O}$) were determined using an isotope ratio mass spectrometer (Delta plus XL) at the Research Institute of Humanity and Nature, Kyoto, Japan. $\delta^{18}\text{O}_c$ was calculated by comparison with Merck cellulose (laboratory working standard), which was inserted after every eighth tree ring cellulose sample during the measurements. The analytical uncertainty for repeated measurements of cellulose was approximately $\pm 0.18\text{‰}$ ($n = 76$).

Climate of the study site

According to the pilot study by Xu et al. (2019b), which analyzed *A. georgei* $\delta^{18}\text{O}_c$ at the same study site (Fig. 1), the annual $\delta^{18}\text{O}_c$ is highly correlated to the local July–August precipitation. To investigate the relationship between seasonal $\delta^{18}\text{O}_c$ and precipitation, regional daily precipitation data (29°N–32°N, 90°E–96°E) based on four stations from the Global Historical Climate Network data set (Menne et al., 2012) were employed. Three out of four meteorological stations ended their records in 1997; therefore, a common period of 1957–1997 was used. The rainy season near the study site lasts from June to September (based on the climatology of 1957–1997; Fig. 2), and this is also the growing season for *A. georgei* (Li et al., 2013; Xu et al., 2019b).

The 5 day mean (pentad) precipitation shown in Figure 2 indicates that the onset of the local monsoonal rainfall occurs around 6.6–87.2 mm, which corresponds to the 29th to 33rd pentad (May 21–June 10). To depict the monsoon onset processes in the study site, we examined the strong-onset years versus the weak-onset years by using 1 SD of the 29th–33rd pentad precipitation as a threshold. The composite precipitation during strong-onset years includes 1960, 1963,

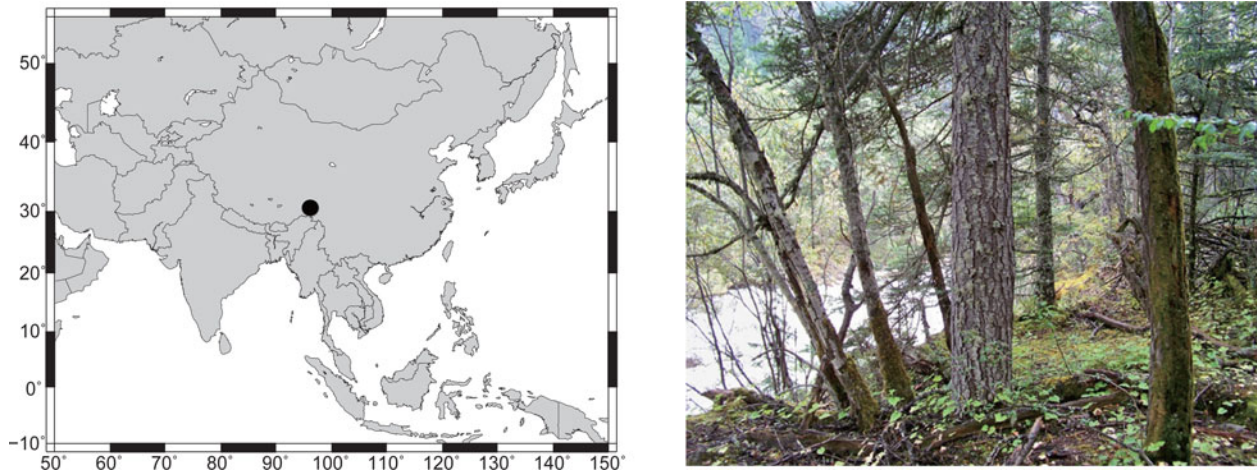


Figure 1. (color online) Map of the sampling site in this study (left) and the sampled *Abies georgei* (right).

1971, 1976, 1977, and 1997; while the weak-onset years are 1958, 1964, 1972, 1983, 1986, and 1995. The 5 day evolution of precipitation during these two groups of years is shown in Figure 2 for the strong and weak onsets. It can be seen that the strong-onset years are equivalent to an early onset, whereas weak-onset years reflect late onset; however, the subsequent amounts of rainfall do not seem to differ throughout the monsoon season. The onset (May 21–June 10) and mature phase (June, July, August) of regional summer monsoons are shown in Figure 2.

Based on strong- and weak-onset years, we plotted the composites of differential winds and precipitable water, which is calculated as the vertical integration of specific humidity for the strong-onset minus weak-onset years using the NCEP/NCAR Reanalysis daily variables (data set from Kalnay et al. 1996), in terms of the low-level (850 hPa)

wind anomalies at $2.5^\circ \times 2.5^\circ$ resolution. These composite maps were done for three periods of 10 days each spanning the onset season, shown in Figure 3. The low-level wind anomalies show a reversal from mid-May to late May, forming a cyclonic circulation over the northern Indian Ocean and the Indian subcontinent, signifying the formation of the monsoon low. By early June, a well-developed monsoonal circulation appears with anomalously strong westerly winds formed over the Arabian Sea into India, before curving northward into the study site on the southeastern Tibetan Plateau. Correspondingly, the precipitable water anomaly increases during late May through early June, supporting the monsoon onset precipitation. These circulation features, as shown in Figure 3, indicate that the variation of monsoon onset in the southeastern Tibetan Plateau is closely connected with the large-scale South Asian monsoon system.

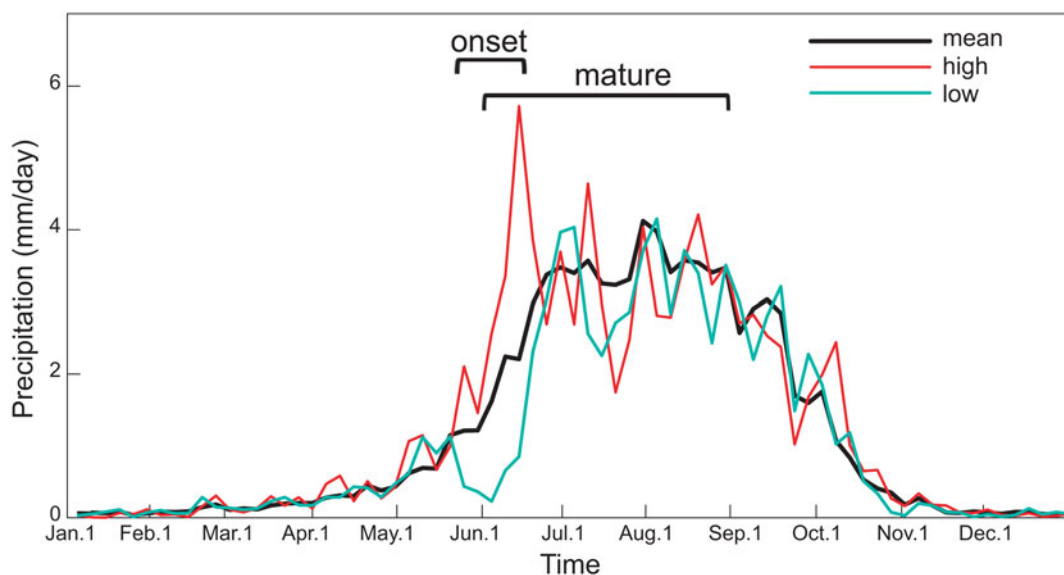


Figure 2. Mean (black line) pentad precipitation covering 29°N – 32°N , 90°E – 96°E from the Global Historical Climate Network during the period of 1957–1997; pentad precipitation at high (red line) and low (green line) precipitation monsoon onset year. (For interpretation of the references to color in this figure legend, the reader is referred to the web version of this article.)

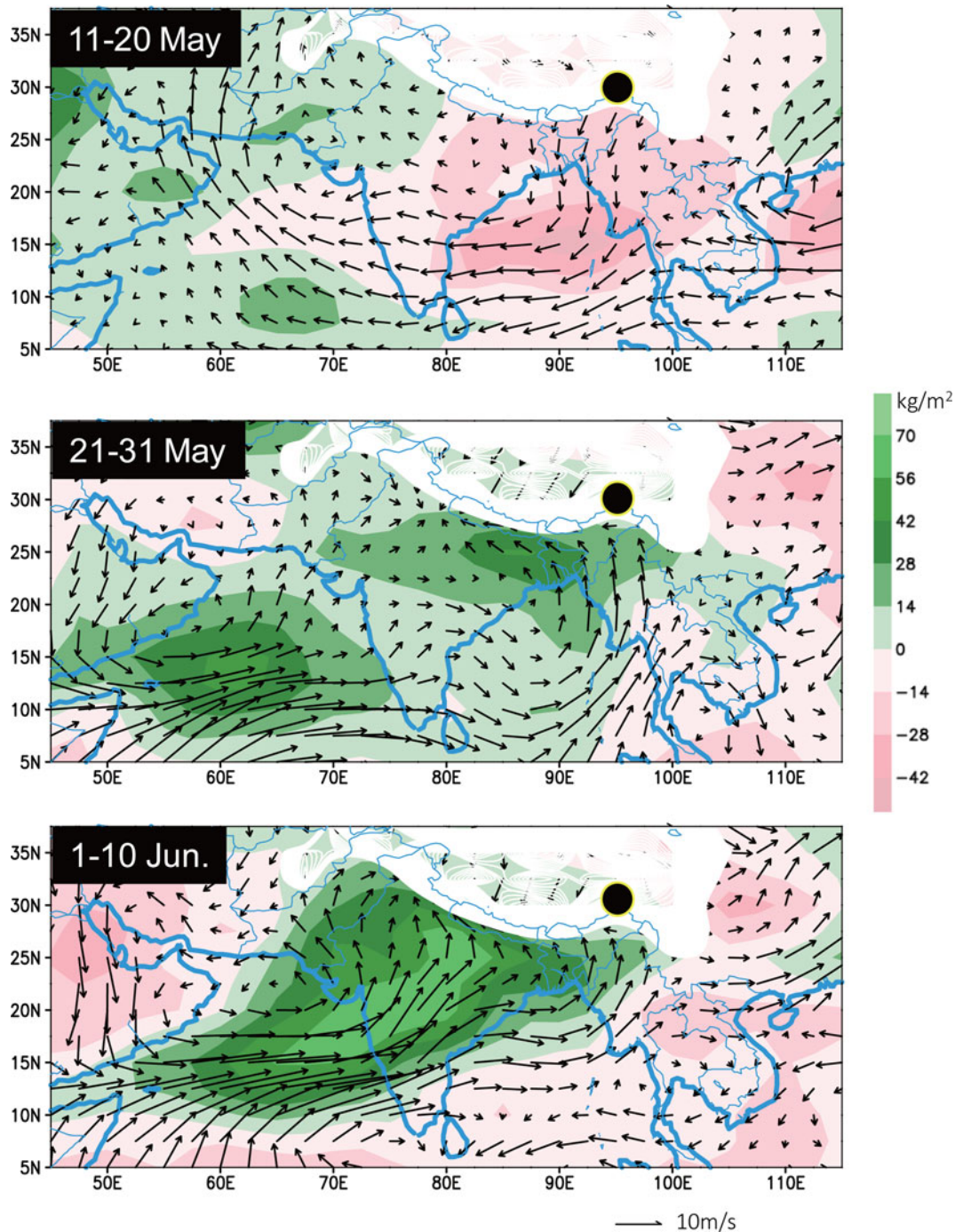


Figure 3. (color online) Composites of anomalous 850 hPa winds (vectors) and precipitable water (shading) between strong and weak monsoon years (based on Fig. 2) during three periods. The study site is indicated by the black dot.

RESULTS AND DISCUSSION

Seasonal tree-ring oxygen isotope variations

When all phases of $\delta^{18}\text{O}_c$ throughout each year during 1950–1980 (Fig. 4a) and 1980–2010 (Fig. 4b) are plotted, it becomes apparent that the S1–S4 segments of $\delta^{18}\text{O}_c$ show a distinct seasonal cycle. The maximum $\delta^{18}\text{O}_c$ occurs in the beginning of the growing season and then decreases throughout the growing season (Fig. 4c). The mean values for S1, S2,

S3, and S4 are 27.60‰, 24.21‰, 21.59‰, and 20.04‰, respectively. A similar seasonal $\delta^{18}\text{O}_c$ pattern that followed seasonal precipitation oxygen isotope and relative humidity changes was also found in *Abies forrestii* in the southeastern Tibetan Plateau (Gao et al., 2013; Zeng et al., 2016, 2017). The correlation coefficients between $\delta^{18}\text{O}_c$ values for S1, S2, S3, S4 and the annual $\delta^{18}\text{O}_c$ are 0.77, 0.87, 0.90, and 0.70, respectively, during 1950–2010. The correlation between S4 ($\delta^{18}\text{O}_c$) in the previous year and S1 in the current

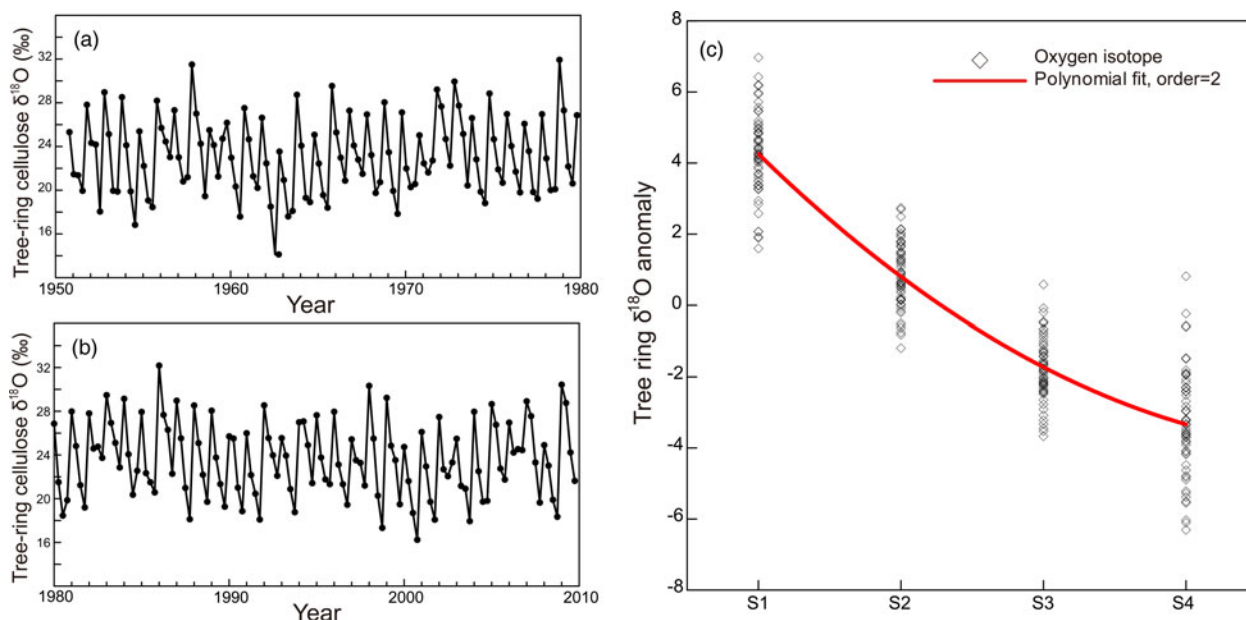


Figure 4. Intra-annual $\delta^{18}\text{O}_c$ time series from *Abies georgei* during the period of 1951–2009.

year is -0.03 ($n = 58$), suggesting that $\delta^{18}\text{O}_c$ in the previous year does not influence $\delta^{18}\text{O}_c$ in the current year (Xu et al., 2018). In addition, the correlation between June–July–August (JJA) precipitation in the previous year and $\delta^{18}\text{O}_c$ of S1 in the current year is not significant ($r = -0.03$, $n = 41$) during the period of 1957–1997, again indicating that monsoon precipitation in the previous year does not affect $\delta^{18}\text{O}_c$ in the current year.

Climatic response of different parts of tree-ring oxygen isotope

It is known that $\delta^{18}\text{O}_c$ formed in different segments of a tree ring records precipitation oxygen isotope and relative humidity at different times of the year (Treydte et al., 2014; Xu et al., 2016; Zeng et al., 2016, 2017). In our study area, the precipitation oxygen isotope is negatively correlated with rainfall and relative humidity during the monsoon season (Gao et al., 2013), with $\delta^{18}\text{O}_c$ depleted when rainfall is high and increased when rainfall is low.

Next, we computed the correlation between S1–S4 $\delta^{18}\text{O}_c$ and pentad precipitation from May to October (Fig. 5). We found that $\delta^{18}\text{O}_c$ of S1 significantly correlates with the late May to mid-June precipitation (29th–33rd pentad) that corresponds to the regional monsoon onset (Fig. 2). The correlation coefficient between S1 ($\delta^{18}\text{O}_c$) and the onset precipitation is -0.69 ($n = 41$, $P < 0.001$). Early monsoon onset is usually associated with decreased precipitation oxygen isotope values and high relative humidity (Tian et al., 2001; Yang et al., 2012), which would further deplete $\delta^{18}\text{O}_c$ of S1 (i.e., when cellulose is formed). Therefore, $\delta^{18}\text{O}_c$ of S1 is a promising proxy for the onset of the regional monsoon rains both statistically and physically.

The Indian summer monsoon (ISM) brings moisture into the southeastern Tibetan Plateau. Precipitation oxygen

isotope as one controlling factor of $\delta^{18}\text{O}_c$ on the southeastern Tibetan Plateau becomes depleted when the ISM onset is early (Tian et al., 2001; Gao et al., 2013). The relationship between ISM onset and $\delta^{18}\text{O}_c$ was found in several individual years (Zeng et al., 2016). To examine the precipitation linkage with the ISM, we compared the relationship between the ISM onset at Kelera (Pai and Nair, 2009) and $\delta^{18}\text{O}_c$ from different segments during the period of 1971–2007 and found that the ISM onset at Kelera is negatively correlated with $\delta^{18}\text{O}_c$ of S1 ($r = -0.36$, $P < 0.01$). These results reveal that $\delta^{18}\text{O}_c$ of S1 records the summer monsoon onset.

$\delta^{18}\text{O}_c$ of S2 shows negative correlations with June and mid-July precipitation, and the June signal is stronger (Fig. 5b). $\delta^{18}\text{O}_c$ of S3 is correlated with July and August precipitation, and July precipitation has a stronger influence on $\delta^{18}\text{O}_c$ of S3 (Fig. 5c). $\delta^{18}\text{O}_c$ of S4 has the strongest correlation with August precipitation. Such negative correlations between $\delta^{18}\text{O}_c$ and precipitation are mainly derived from negative correlations between precipitation amount and precipitation oxygen isotope, as is evident for monsoon season precipitation on the southeastern Tibetan Plateau (Tian et al., 2001; Yang et al., 2012; Gao et al., 2013).

In summary, regional monsoon onset and mature-phase precipitation (as outlined in Fig. 2) have the highest correlations with $\delta^{18}\text{O}_c$ of S1 and averaged $\delta^{18}\text{O}_c$ of S2, S3, and S4, respectively (Table 1). In addition, precipitation in June, July, and August showed the strongest correlation with $\delta^{18}\text{O}_c$ of S2, S3, and S4, respectively (Table 1). Although the seasonal $\delta^{18}\text{O}_c$ data are based on one tree, the monsoon onset/mature-phase precipitation and monthly precipitation signal from seasonal $\delta^{18}\text{O}_c$ using one tree is stronger than from annual $\delta^{18}\text{O}_c$ using four trees (Table 1). Compared with annual $\delta^{18}\text{O}_c$, seasonal $\delta^{18}\text{O}_c$ variations provide not only more detailed climatic information but also a stronger climatic signal.

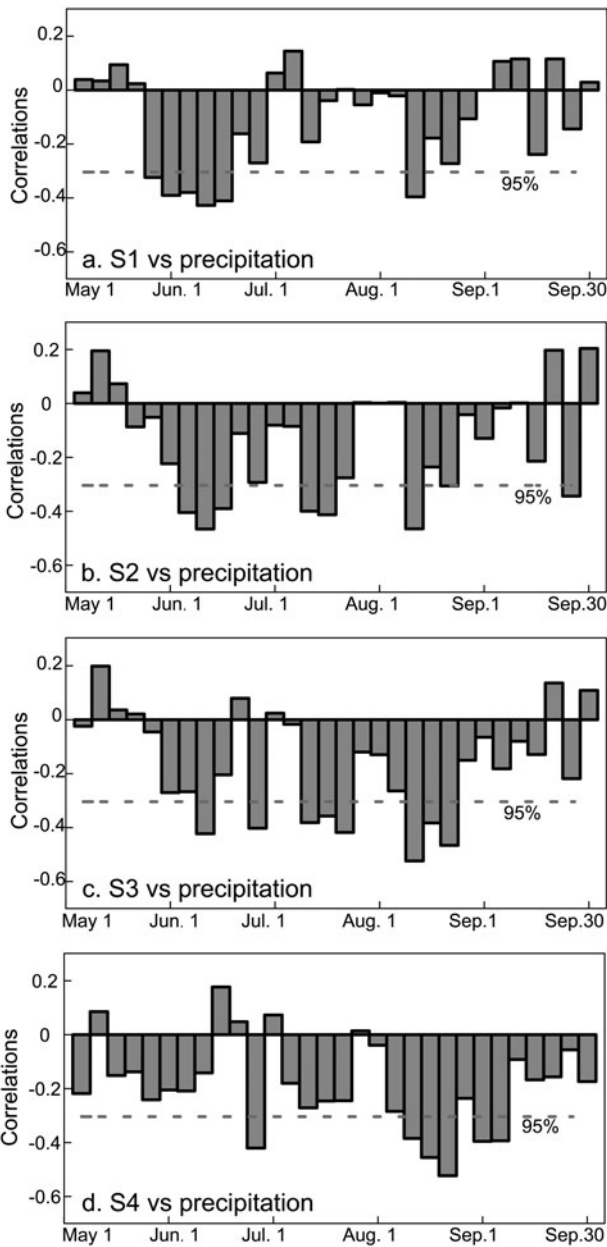


Figure 5. Correlations between S1–S4 $\delta^{18}\text{O}_c$ and pentad precipitation from May to September during the period of 1957–1997; the dashed line indicates the 95% confidence level.

Reconstruction of precipitation for monsoon onset and mature phase

Given the aforementioned analysis, regional monsoon onset can be reconstructed based on a linear relationship with $\delta^{18}\text{O}_c$ of S1. We examined the mature phase of the monsoon precipitation (JJA) by reconstructing it using the combination of S2, S3, and S4. We constructed a set of linear regression models between monsoon onset and mature-phase precipitation and $\delta^{18}\text{O}_c$ from different segments:

$$\text{PRE}_{\text{onset}} = -7.76 * \text{S1} + 252.88 \quad (R^2 = 0.48, n = 41, P < 0.001)$$

$$\text{PRE}_{\text{mature}} = -10.2 * (\text{S2} + \text{S3} + \text{S4}) + 964.49 \quad (R^2 = 0.67, n = 41, P < 0.001)$$

Here, $\text{PRE}_{\text{onset}}$ and $\text{PRE}_{\text{mature}}$ represent regional monsoon onset and mature-phase precipitation, respectively. S1 to S4 represent $\delta^{18}\text{O}_c$ values from segments S1 to S4. Split calibration–verification tests for monsoon onset and mature-phase precipitation reconstruction are shown in Tables 2 and 3, respectively. For both subperiods of monsoon onset and mature-phase precipitation, most rigorous statistics, such as reduction of error (RE) and coefficient of efficiency (CE) are positive, suggesting the reconstruction is robust (Cook et al., 1999). The observed and reconstructed monsoon onset and mature-phase precipitation showed consistent variations at interannual and decadal scales (Fig. 6). The long-term seasonal $\delta^{18}\text{O}_c$ data set covering several decades showed the fidelity of monsoon onset and mature-phase precipitation reconstruction based on seasonal $\delta^{18}\text{O}_c$.

As a further validation, we used the reconstructed onset precipitation (as in Fig. 6a) to produce a regression map of low-level winds and precipitable water during the May 21 through June 10 period, corresponding to Figure 3. The regressed low-level atmospheric circulations with the onset precipitation reconstruction (Fig. 7) reveals a pattern similar to the strong-onset minus weak-onset composite in early June (Fig. 3), indicating increased monsoonal westerly winds and the deepened monsoonal trough over the India

Table 1. Correlations between precipitation and tree-ring $\delta^{18}\text{O}$ from parts S1 to S4 and annual(4).

Correlations	S1	S2	S3	S4	S2–4 ^a	Annual(4) ^b
Onset	-0.69*	-0.59*	-0.43*	-0.15	-0.45*	-0.50*
JJA(June-July-August)	-0.45*	-0.68*	-0.77*	-0.65*	-0.82*	-0.78*
June	-0.58*	-0.63*	-0.42*	-0.16	-0.46*	-0.51*
July	-0.06	-0.44*	-0.53*	-0.36	-0.52*	-0.49*
August	-0.30	-0.36	-0.57*	-0.68*	-0.63*	-0.55*

^aS2–4 indicates average of S2, S3, and S4.

^bAnnual(4): the annual $\delta^{18}\text{O}_c$ chronology based on four trees (XC2, XC6, XC12, and XC14) that was produced by Xu et al. (2019b).

* $P < 0.01$.

bold type indicates the highest correlations between precipitation and tree-ring $\delta^{18}\text{O}$ from parts S1 to S4 and annual(4).

Table 2. Calibration and verification statistics for monsoon onset precipitation reconstruction.

Calibration period	r	R^2	Verification period	RE ^a	CE ^b
Full period (1957–1997)	−0.69	0.48		—	—
Early half (1957–1976)	−0.75	0.56	Late half (1977–1997)	0.49	0.49
Late half (1977–1997)	−0.64	0.41	Early half (1957–1976)	0.29	0.29

^aRE, reduction of error.^bCE, coefficient of efficiency.**Table 3.** Calibration and verification statistics for monsoon mature-phase (JJA) precipitation reconstruction.

Calibration period	r	R^2	Verification period	RE ^a	CE ^b
Full period (1957–1997)	−0.82	0.67		—	—
Early half (1957–1976)	−0.89	0.79	Late half (1977–1997)	0.81	0.78
Late half (1977–1997)	−0.75	0.56	Early half (1957–1976)	0.60	0.55

^aRE, reduction of error.^bCE, coefficient of efficiency.

subcontinent. This is another line of evidence that the tree ring $\delta^{18}\text{O}_c$ -recorded onset precipitation signal in the southeastern Tibetan Plateau is closely associated with the large-scale South Asian monsoon variation.

Seasonal $\delta^{18}\text{O}_c$ from one tree showed great potential for robust monsoon onset reconstruction, which cannot be done using annual $\delta^{18}\text{O}_c$ from four trees. Moreover, monthly precipitation reconstruction has been considered challenging when it comes to the analysis of annual tree-ring proxies; however, we found applicability based on the negative

correlation between August precipitation and $\delta^{18}\text{O}_c$ of S4 (Table 1). It should be noted that building a $\delta^{18}\text{O}_c$ record based on a single tree should be treated cautiously. Two or more trees should be included for cross-checking purposes. Increased sampling resolution per year (e.g., six or eight segments per year) may allow us to extract a stronger and more accurate monthly precipitation signal. However, the exponential increase in the cost of analysis as the sampling resolution increases can be prohibitive.

Considering that tree-ring oxygen isotopes record monsoon season moisture variations in monsoonal Asia, seasonal $\delta^{18}\text{O}_c$ analysis in monsoonal Asia will shed more light on the Asian summer monsoon variability for the long term. For example, seasonal $\delta^{18}\text{O}_c$ -based monsoon onset and mature-phase precipitation reconstruction at different locations in monsoonal Asia can provide a spatial variation of the different phases of monsoon precipitation during the past several hundred years. Millennial seasonal $\delta^{18}\text{O}_c$ records in monsoonal Asia can potentially reveal external forcing (such as solar activity, greenhouse gases) and internal forcing (such as ENSO) influences on monsoon precipitation. Seasonal $\delta^{18}\text{O}_c$ chronologies in monsoonal Asia in a past warm period (such as the mid-Holocene) can be useful to understand possible precipitation changes in the context of global warming.

CONCLUSIONS

In this study, we took a novel step, dividing the seasonal tree-ring oxygen isotope in one tree ring from the southeastern Tibetan Plateau into four segments (S1 to S4) and analyzing the segments for the period of 1951–2009. We found that $\delta^{18}\text{O}_c$ of S1 has the strongest correlations with the regional monsoon onset precipitation, while $\delta^{18}\text{O}_c$ values for S2, S3, and S4 correlate strongly with the June, July, and August precipitation, respectively. The linear regression models between $\delta^{18}\text{O}_c$ of S1 and monsoon onset precipitation and $\delta^{18}\text{O}_c$

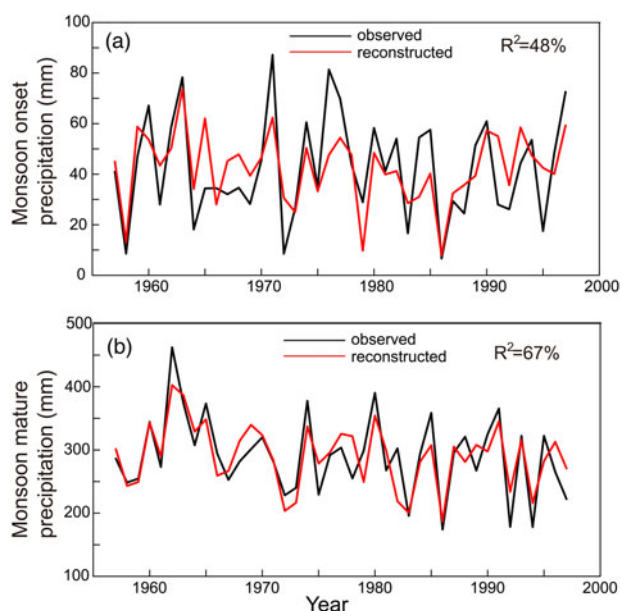


Figure 6. Comparison of the reconstructed JJA precipitation (red line) and precipitation data (black line) from Global Historical Climate Network during the period of 1957–1997. (For interpretation of the references to color in this figure legend, the reader is referred to the web version of this article.)

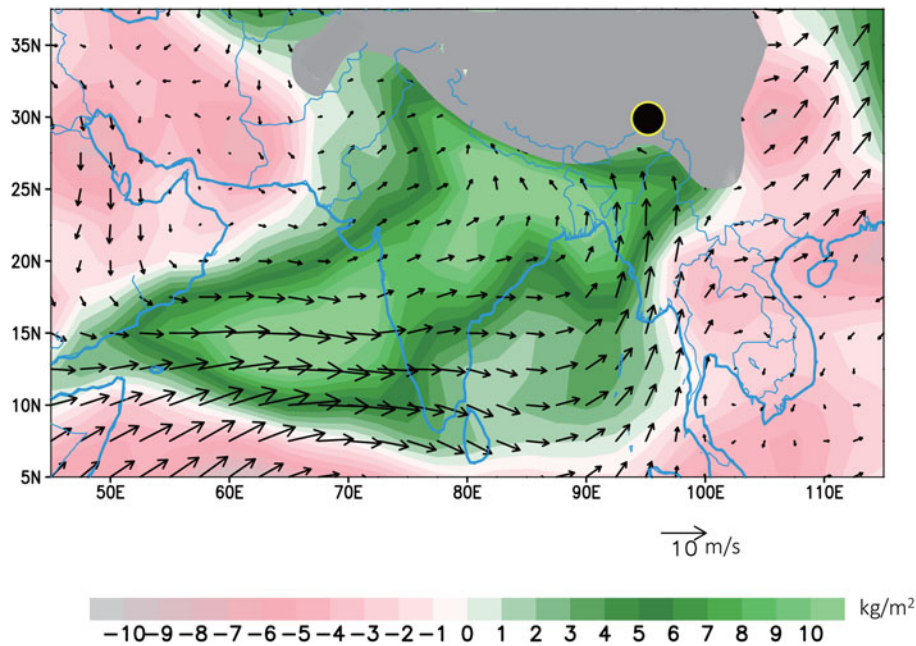


Figure 7. (color online) Anomalous winds at 850 hPa and precipitable water during May 21–June 10 regressed on the reconstructed onset precipitation (normalized) from 1957 to 1997 based on the NCEP/NCAR Reanalysis data set (Kalnay et al., 1996). Anomalous wind speed greater than 3 m/s and precipitable water greater than 4.5 kg/m² are significant ($P < 0.05$). Study site is indicated as black dot.

S2–S4 and monsoon mature-phase precipitation pass all statistical tests commonly used for calibration and verification. The results suggest that using seasonal $\delta^{18}\text{O}_c$ from one tree alone can achieve robust monsoon onset and monthly precipitation reconstruction, a task that is difficult using only annual $\delta^{18}\text{O}_c$ and tree-ring width variations. Future studies should consider using seasonal $\delta^{18}\text{O}_c$ collected at different sites throughout monsoonal Asia to reconstruct the distinct monsoon life cycle as revealed in daily precipitation for a better understanding of variation of the South Asia summer monsoon in the pre-instrumental period.

ACKNOWLEDGMENTS

This study was supported by the National Natural Science Foundation of China, grants 41888101, 41630529, 41672179, 41671193, 41430531, and 41690114; the National Key R&D Program of China, grant 2017YFE0112800; the Chinese Academy of Sciences (CAS) Pioneer Hundred Talents Program; and the Strategic Priority Research Program of the Chinese Academy of Sciences, grants XDB26020000 and XDA13010106. SYW is supported by a U.S. DOE HyperFACET grant. We deeply appreciate helpful comments from the editors and two anonymous reviewers that improved the article.

REFERENCES

- Cleaveland, M.K., Stahle, D.W., Therrell, M.D., Villanueva-Diaz, J., Burns, B.T., 2003. Tree-ring reconstructed winter precipitation and tropical teleconnections in Durango, Mexico. *Climatic Change* 59, 369–388.
- Cook, E.R., Meko, D.M., Stahle, D.W., Cleaveland, M.K., 1999. Drought reconstructions for the continental United States. *Journal of Climate* 12, 1145–1162.
- Dansgaard, W., 1964. Stable isotopes in precipitation. *Tellus* 16, 436–468.
- Gao, J., Masson-Delmotte, V., Risi, C., He, Y., Yao, T., 2013. What controls precipitation $\delta^{18}\text{O}$ in the southern Tibetan Plateau at seasonal and intra-seasonal scales? A case study at Lhasa and Nyalam. *Tellus B: Chemical and Physical Meteorology* 65, 21043.
- Grießinger, J., Bräuning, A., Helle, G., Thomas, A., Schleser, G., 2011. Late Holocene Asian summer monsoon variability reflected by $\delta^{18}\text{O}$ in tree-rings from Tibetan junipers. *Geophysical Research Letters* 38, L03701.
- Griffin, D., Woodhouse, C.A., Meko, D.M., Stahle, D.W., Faulstich, H.L., Carrillo, C., Touchan, R., Castro, C.L., Leavitt, S.W., 2013. North American monsoon precipitation reconstructed from tree-ring latewood. *Geophysical Research Letters* 40, 954–958.
- Joseph, P.V., Eischeid, J.K., Pyle, R.J., 1994. Interannual variability of the onset of the Indian summer monsoon and its association with atmospheric features, El Niño, and sea surface temperature anomalies. *Journal of Climate* 7, 81–105.
- Kalnay, E., Kanamitsu, M., Kistler, R., et al., 1996. The NCEP/NCAR 40-year reanalysis project. *Bulletin of the American Meteorological Society* 77, 437–472.
- Krishnan, R., Ramesh, K.V., Samala, B.K., Meyers, G., Slingo, J.M., Fennessy, M.J., 2006. Indian Ocean-monsoon coupled interactions and impending monsoon droughts. *Geophysical Research Letters* 33(8), 08711.
- Kulkarni, A., Kripalani, R., Sabade, S., Rajeevan, M., 2011. Role of intra-seasonal oscillations in modulating Indian summer monsoon rainfall. *Climate Dynamics* 36, 1005–1021.
- Kurita, N., Ichiyangi, K., Matsumoto, J., Yamanaka, M., Ohata, T., 2009. The relationship between the isotopic content of

- precipitation and the precipitation amount in tropical regions. *Journal of Geochemical Exploration* 102, 113–122.
- Li, R., Wang, S. Y., Gillies, R. R., Buckley, B. M., Yoon, J. H., Cho, C., 2019. Regional trends in early-monsoon rainfall over Vietnam and CCSM4 attribution. *Climate Dynamics* 52, 363–372.
- Li, X., Liang, E., Gričar, J., Prislán, P., Rossi, S., Čufar, K., 2013. Age dependence of xylogenes and its climatic sensitivity in Smith fir on the south-eastern Tibetan Plateau. *Tree Physiology* 33, 48–56.
- Managave, S., Sheshshayee, M., Bhattacharyya, A., Ramesh, R., 2010a. Intra-annual variations of teak cellulose $\delta^{18}\text{O}$ in Kerala, India: implications to the reconstruction of past summer and winter monsoon rains. *Climate Dynamics* 37, 555–567.
- Managave, S., Sheshshayee, M., Borgaonkar, H., Ramesh, R., 2010b. Past break-monsoon conditions detectable by high resolution intra-annual $\delta^{18}\text{O}$ analysis of teak rings. *Geophysical Research Letters* 37, L05702.
- Menne, M.J., Durre, I., Vose, R.S., Gleason, B.E., Houston, T.G., 2012. An overview of the Global Historical Climatology Network—Daily Database. *Journal of Atmospheric and Oceanic Technology* 29, 897–910.
- Pai, D., Nair, R.M., 2009. Summer monsoon onset over Kerala: new definition and prediction. *Journal of Earth System Science* 118, 123–135.
- Roden, J.S., Lin, G., Ehleringer, J.R., 2000. A mechanistic model for interpretation of hydrogen and oxygen isotope ratios in tree-ring cellulose. *Geochimica et Cosmochimica Acta* 64, 21–35.
- Sano, M., Tshering, P., Komori, J., Fujita, K., Xu, C., Nakatsuka, T., 2013. May–September precipitation in the Bhutan Himalaya since 1743 as reconstructed from tree ring cellulose $\delta^{18}\text{O}$. *Journal of Geophysical Research: Atmospheres* 118, 8399–8410.
- Shao, X., Huang, L., Liu, H., Liang, E., Fang, X., Wang, L., 2005. Reconstruction of precipitation variation from tree rings in recent 1000 years in Delingha, Qinghai. *Science in China, Series D: Earth Science* 48, 939–949.
- Siingh, D., Buchunde, P.S., Gandhi, H., Singh, R., Singh, S., Patil, M.N., Singh, R.P., 2015. Lightning and convective rain over Indian peninsula and Indo-China peninsula. *Advances in Space Research* 55, 1085–1103.
- Tian, L., Masson-Delmotte, V., Stievenard, M., Yao, T., Jouzel, J., 2001. Tibetan Plateau summer monsoon northward extent revealed by measurements of water stable isotopes. *Journal of Geophysical Research: Atmospheres* 106, 28081–28088.
- Touchan, R., Akkemik, Ü., Hughes, M.K., Erkan, N., 2007. May–June precipitation reconstruction of southwestern Anatolia, Turkey during the last 900 years from tree rings. *Quaternary Research* 68, 196–202.
- Treydte, K., Boda, S., Graf Pannatier, E., Fonti, P., Frank, D., Ullrich, B., Saurer, M., Siegwolf, R., Battipaglia, G., Werner, W., 2014. Seasonal transfer of oxygen isotopes from precipitation and soil to the tree ring: source water versus needle water enrichment. *New Phytologist* 202, 772–783.
- Treydte, K.S., Schleser, G.H., Helle, G., Frank, D.C., Winiger, M., Haug, G.H., Esper, J., 2006. The twentieth century was the wettest period in northern Pakistan over the past millennium. *Nature* 440, 1179–1182.
- Ullah, K., Shouting, G., 2013. A diagnostic study of convective environment leading to heavy rainfall during the summer monsoon 2010 over Pakistan. *Atmospheric Research* 120, 226–239.
- Vuille, M., Bradley, R., Werner, M., Healy, R., Keimig, F., 2003. Modeling $\delta^{18}\text{O}$ in precipitation over the tropical Americas: 1. Interannual variability and climatic controls. *Journal of Geophysical Research: Atmospheres* 108, 4174.
- Wang, P., Wang, B., Cheng, H., et al., 2017. The global monsoon across time scales: mechanisms and outstanding issues. *Earth-Science Reviews* 174, 84–121.
- Wang, S., Davies, R., Huang, W., Gillies, R., 2011. Pakistan's two-stage monsoon and links with the recent climate change. *Journal of Geophysical Research: Atmospheres* 116, D16114.
- Wang, S., Lin, Y., Wu, C., 2016. Interdecadal change of the active-phase summer monsoon in East Asia (Meiyu) since 1979. *Atmospheric Science Letters* 17, 128–134.
- Xu, C., Pumijumong, N., Nakatsuka, T., Sano, M., Guo, Z., 2018. Inter-annual and multi-decadal variability of monsoon season rainfall in central Thailand during the period 1804–1999, as inferred from tree ring oxygen isotopes. *International Journal of Climatology* 38, 5766–5776.
- Xu, C., Pumijumong, N., Nakatsuka, T., Sano, M., Li, Z., 2015. A tree-ring cellulose $\delta^{18}\text{O}$ -based July–October precipitation reconstruction since AD 1828, northwest Thailand. *Journal of Hydrology* 529, 433–441.
- Xu, C., Sano, M., Nakatsuka, T., 2011. Tree ring cellulose $\delta^{18}\text{O}$ of *Fokienia hodginsii* in northern Laos: a promising proxy to reconstruct ENSO? *Journal of Geophysical Research* 116, D24109.
- Xu, C., Shi, J., Zhao, Y., Nakatsuka, T., Sano, M., Shi, S., Guo, Z., 2019a. Early summer precipitation in the lower Yangtze River basin for AD 1845–2011 based on tree-ring cellulose oxygen isotopes. *Climate Dynamics* 52, 1583–1594.
- Xu, C., Zheng, H., Nakatsuka, T., Sano, M., 2013. Oxygen isotope signatures preserved in tree ring cellulose as a proxy for April–September precipitation in Fujian, the subtropical region of south-east China. *Journal of Geophysical Research: Atmospheres* 118, 12,805–12,815.
- Xu, C., Zheng, H., Nakatsuka, T., Sano, M., Li, Z., Ge, J., 2016. Inter- and intra-annual tree-ring cellulose oxygen isotope variability in response to precipitation in Southeast China. *Trees* 30, 785–794.
- Xu, C., Zhu, H., Nakatsuka, T., Sano, M., Li, Z., Shi, F., Liang, E., Guo, Z., 2019b. Sampling strategy and climatic implication of tree-ring cellulose oxygen isotopes of *Hippophae tibetana* and *Abies georgei* on the southeastern Tibetan Plateau. *International Journal of Biometeorology* 63, 679–686.
- Yang, B., Qin, C., Wang, J., He, M., Melvin, T., Osborn, T., R, B., 2014. A 3,500-year tree-ring record of annual precipitation on the northeastern Tibetan Plateau. *Proceedings of the National Academy of Sciences USA* 111, 2903–2908.
- Yang, X., Yao, T., Yang, W., Xu, B., He, Y., Qu, D., 2012. Isotopic signal of earlier summer monsoon onset in the Bay of Bengal. *Journal of Climate* 25, 2509–2516.
- Young, G.H., Loader, N.J., McCarroll, D., Bale, R.J., Demmler, J.C., Miles, D., Whitney, M., 2015. Oxygen stable isotope ratios from British oak tree-rings provide a strong and consistent record of past changes in summer rainfall. *Climate Dynamics* 45, 3609–3622.
- Zeng, X., Liu, X., Evans, M.N., Wang, W., An, W., Xu, G., Wu, G., 2016. Seasonal incursion of Indian monsoon humidity and precipitation into the southeastern Qinghai–Tibetan Plateau inferred from tree ring $\delta^{18}\text{O}$ values with intra-seasonal resolution. *Earth and Planetary Science Letters* 443, 9–19.
- Zeng, X., Liu, X., Treydte, K., Evans, M.N., Wang, W., An, W., Sun, W., Xu, G., Wu, G., Zhang, X., 2017. Climate signals in tree-ring $\delta^{18}\text{O}$ and $\delta^{13}\text{C}$ from southeastern Tibet: insights from observations and forward modelling of intra- to interdecadal variability. *New Phytologist* 216, 1104–1118.